

Original Article

# Investigation of Low-Temperature Desalination Process by Flashing, PV-Thermal, Thermal Storage, and Magnetized Nanofluids

Samuel Sami Howard<sup>1,2</sup>

<sup>1</sup>Tras Pacific Energy, Inc., Las Vegas, Nevada, USA

<sup>2</sup>North Dakota University, Grand Forks, ND, USA

Received: 26 December 2022

Revised: 30 January 2023

Accepted: 09 February 2023

Published: 16 February 2023

**Abstract** - Modeling of the PV-thermal solar collector and thermal storage PCM using magnetized nanofluids to power the multi-stage flashing chambers to desalinate seawater has been presented. The proposed model was established after the mass and energy conservation equations were written for finite control volume with properties of the magnetized nanofluids heat transport fluid. The magnetized nanofluids studied and presented hereby are  $\text{Al}_2\text{O}_3$ ,  $\text{CuO}$ ,  $\text{Fe}_3\text{O}_4$ , and  $\text{SiO}_2$ . At different magnetic fields up to 3000 Gauss, the multiple chamber flashing process has been studied under various conditions, including different solar radiations, brine flows and concentrations, nanofluids concentrations, and flashing chamber temperatures and pressures. Solar radiations were taken as 500 w/m<sup>2</sup>, 750 w/m<sup>2</sup>, 1000 w/m<sup>2</sup>, and finally, 1200 w/m<sup>2</sup>. Nanofluids volumetric concentrations considered varied from 1% to 20%. There is clear evidence that the higher the solar radiation, the higher the flashed flow produced. The results also clearly showed that the irreversibility is reduced by using magnetized nanofluid  $\text{Al}_2\text{O}_3$  at higher concentrations of 10% to 20% compared to water as base fluid. The highest irreversibility was experienced when water was used as a base fluid, and the lowest irreversibility was associated with nanofluid  $\text{SiO}_2$ . The irreversibility increase depends upon the type of nanofluid and its thermodynamic properties. Furthermore, the higher the concentration, 10% to 20% of  $\text{Al}_2\text{O}_3$ , the higher the availability at the last flashing chamber. However, the availability is progressively reduced at the last flashing chamber. Finally, the predicted results were compared well with experimental data published in the literature.

**Keywords** - Desalination, flashing chamber, PV Thermal, Thermal Storage, Magnetized Nanofluids, Numerical Model, validation.

## 1. Introduction

It is well known and has been reported by references [1-11] that Remote coastal areas in the Middle East, Africa, Mediterranean, and Caribbean islands are suffering from an acute shortage of drinking water. It is also anticipated that by the year 2025, more than 60% of the world's population will suffer from serious drinking water shortages [1-3]. As more places face water scarcity, desalination is considered a possible answer. However, energy and financial requirements limit how widely that process can be used. Conventional desalination techniques, such as multi-stage flash desalination (MSF), vapor compression (VC), reverse osmosis (RO), membrane distillation (MD), and electro dialysis (ED), require significant thermal energy to drive. We believe solar energy is the logical response to these limitations and can power thermal and electrical desalination systems. It was shown by references [3,6] that solar desalination can be achieved in areas with high solar intensity and a lack of fresh water drinking.

Nannaronea et al. [31] presented a general model to simulate the Multiple Stage Flash distillation, MSF process.

The model was implemented within the Camel-Pro™ Process Simulator. Several validation tests were conducted to confirm that a model is an efficient tool for MSF plants' design and prediction of the most important variables in the MSF process. Lumped parameter dynamic models were developed in Al-Fulaij's PhD thesis [8] or the once-through (MSF-OT) and the brine circulation (MSF-BC) processes. The models were coded using the PROMS modeling program. The model predictions for both MSF-OT and MSF-BC in steady-state and dynamic conditions showed good agreement against data from existing MSF plants with an error of less than 1.5%. Reference [9], the proposed methodology provides a set of modular simulations of components that allow the creation of complex models used to optimise the full water desalination supply chain. The optimization scheme included mathematical programming (MP) models that an external MP solver solves for Saudi Arabia, which is considered the worldwide leader in desalinated water capacity.

An integrated system that uses a flashing desalination technique coupled with a nano-fluid-based solar collector as



a heat source has been presented by Hala [13] to study both the effect of different operating modes and of the variation of functioning parameters and weather conditions on the freshwater production using nanofluid. The flashing unit is performed by a similar construction design technique to commercial multi-stage flashing (MSF) plant. Another objective of the reported mathematical model developed was calculating the system's productivity under different operating conditions.

A mathematical model for a multi-stage flash (MSF) desalination system with brine recirculation (BR) configuration has been developed and presented by reference [14]. The heat source for BR-MSF was described as chosen as a nanofluid-based direct absorption solar collector (DASC), where the numerical model was developed. Both these systems, BR-MSF and DASC, were coupled via a counter-current flow heat exchanger. The overall performance of the combined system was determined in terms of gained output ratio, referred to as (GOR). The conceptual design for a photovoltaic thermal (PV/T) solar panel has been developed and analyzed to control the inherent temperature increase of PV cells to increase electrical efficiency [15-18]. A hybrid solar panel has been developed and presented by Yang et al. [1] and Sami [17,18] to integrate photovoltaic (PV) cells onto a substrate through a functionally graded material (FGM) with water tubes cast inside, through which water serves as both heat sink and solar heat collector.

Recently, Sami [3] presented mathematical and numerical modeling of the photovoltaic (PV)-thermal solar system to power the multi-stage flashing chamber process is presented. The proposed model was established after the mass and energy conservation equations written for finite control volume were integrated with the properties of the water and nanofluids. The nanofluids studied were  $Ai_2O_3$ ,  $CuO$ ,  $Fe_3O_4$ , and  $SiO_2$ . The multiple flashing chamber process was studied under various conditions, including direct solar radiation levels, brine flows and concentrations, and nanofluid concentrations. The nanofluid volumetric concentrations considered varied from 1% to 20%. There is clear evidence that the higher the solar radiation, the higher the flash flow produced. The results also clearly show that irreversibility is reduced by using nanofluid  $Ai_2O_3$  at higher concentrations of 10% to 20% compared to water as the base fluid. The highest irreversibility was experienced when water was used as a base fluid, and the lowest irreversibility was associated with nanofluid  $SiO_2$ . The irreversibility increase depends upon the type of nanofluid and its thermodynamic properties—furthermore, the higher the concentration, the higher the availability at the last flashing chamber. However, the availability is progressively at the last reduced flashing chamber. Finally, the predicted results compare well with experimental data published in the literature.

Therefore, this research has been undertaken to study the impact of solar energy and magnetized nanofluids on the desalination process. Thermal and membrane desalination were focused on the evaporation processes using steam. The novel concept presented in this paper on the MSF is an extension of the work presented by Sami [3], where the PV-Thermal solar panels use hot heat transfer fluid with magnetized nanofluids in the MSF process. The main objective of this paper is to present mathematical and numerical modeling using nanofluids and PV-thermal solar to power the multi-stage flashing chamber thermal process. The proposed model has been established after the mass and energy conservation equations of the flashing process integrated with the vapor and magnetized nanofluids' thermal and thermophysical properties at different volume fractions and solar radiation. The magnetized nanofluids studied are  $Ai_2O_3$ ,  $CuO$ ,  $Fe_3O_4$ , and  $SiO_2$  at different volume fractions. The process of multi-stage flashing using PV-Thermal solar panels and nanofluids has been analyzed under different conditions of seawater (brine) salt concentration, brine flows, temperatures, and nanofluids concentration as solar radiations.

## 2. Numerical Modeling

### 2.1. PV Model

The solar photovoltaic panel is constructed of various modules, and each module consists of arrays and cells. The dynamic current output can be obtained as follows [15-18];

$$I_p = I_L - I_o \left[ \exp \left( \frac{q(V + I_p R_s)}{A k T_c} - \frac{V + I_p R_s}{R_{sh}} \right) \right] \quad (1)$$

- $I_p$ : Output current of the Pv module
- $I_L$ : Light-generated current per module
- $I_o$ : Reverse saturation current per module
- $V$ : Terminal voltage per module
- $R_s$ : Diode series resistance per module
- $R_{sh}$ : Diode shunt resistance per module
- $q$ : Electric charge
- $k$ : The Boltzmann constant
- $A$ : Diode ideality factor for the module

$$P(t) = 1.73 \eta V I \cos(\theta) \quad (2)$$

Where;  $\eta$  is the efficiency of PV,  $V$  and  $I$  represent output voltage and amperage, and  $\theta$  is the phase angle.

### 2.2. PV-Thermal Model

It is assumed in this model that all PV cells behave the same; therefore, this model can be applied to the whole PV solar panel. This model is an extension of the work presented by Sami and Campoverde [18], that the thermal heat absorbed by the PV solar cell can be calculated by the following equation.

**Table. 1 Thermophysical Properties of magnetized nanofluids**

	<b>Ai<sub>2</sub>O<sub>3</sub></b>	<b>CuO</b>	<b>Fe3O4</b>	<b>SiO<sub>2</sub></b>
<b>C<sub>p nf</sub></b>	b = 0.1042a + 6226.5	b = 0.2011a + 5730.8	b = 0.8318a + 4269.8	b = 0.6187a + 4293.2
<b>K<sub>nf</sub></b>	b = 2E-05a + 1.4888	b = 5E-05a + 1.3703	b = 0.0002a + 1.0209	b = 0.0001a + 1.0265
<b>h</b>	b = 0.0031a + 73.092	b = 0.0031a + 73.073	b = 0.003a + 73.225	b = 0.003a + 73.231

$$Q_{in} = \alpha_{abs}GS_p \quad (3)$$

Where

- $\alpha_{abs}$ : Overall absorption coefficient
- G: Total Solar radiation incident on the PV module
- $S_p$ : Total area of the PV module

Meanwhile, the PV cell Temperature is computed from the following heat balance as per Sami and Martin [18];

$$mC_{p\_module} \frac{dT_c}{dt} = Q_{in} - Q_{conv} - Q_{elect} \quad (4)$$

Where.

- $T_c$ : PV Cell Temperature
- $mC_{p\_module}$ : Thermal capacity of the PV module
- t: time
- $Q_{in}$ : Energy received due to solar irradiation,
- $Q_{conv}$ : Energy loss due to Convection
- $Q_{elect}$ : Electrical power generated

Interested readers in the detailed calculations of the terms of the above equation are advised to consult references [18, 19].

### 3. Multi-stage Flashing Chamber Model

This section presents the mathematical and numerical modeling of the new concept using an integrated, magnetized nanofluids loop, thermal storage tank, and PV-thermal solar collector to drive the multi-stage flashing chamber thermal (MSF) process as shown in the Figures. 1 and 2. to generate a desalination system. In these figures, the brine is preheated by the nanofluid circulating in the PV-thermal loop, where the dissipated heat from the PV solar panel is absorbed, as shown in the figure. The flashing process occurs in the flashing chamber where the flashed vapor is generated and condensed on the heat exchanger cooled down by the incoming brine flow. The distilled condensed vapor is collected, and the brine flow is circulated to the next flashing chamber, where the same flashing process is repeated. The model proposed has been established after the mass and energy equations coupled with the state equations for the nanofluids and water as base fluid at different solar radiations. This numerical process has been repeated for each of the flashing chambers. In the following, we present the mass and energy equations of the flow in the flashing chamber.

Each flashing chamber is considered a discrete control volume and has a constant volume; therefore, by applying the

first law of thermodynamics to the control volume, the mass balance and energy balance across the flashing chamber can be given by the mass and energy balance equations given in reference [7]. Interested readers are advised to consult Mohamed Qiblawey and Fawzi Banat.[7] and Sami[3].

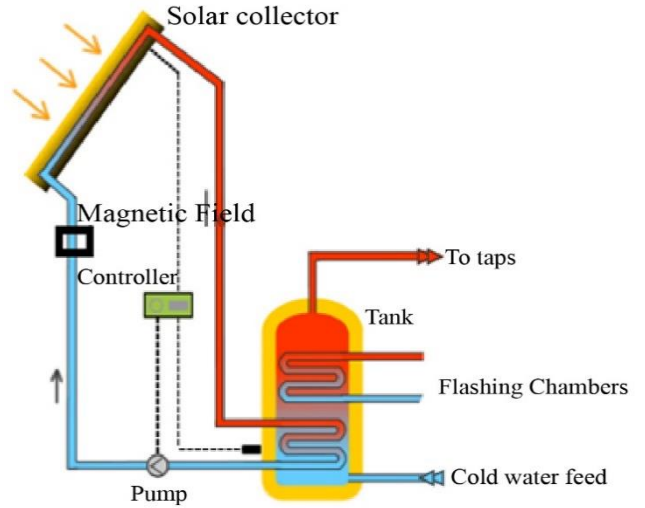


**Fig. 1 PV-Thermal Integrated Thermal Storage to feed the Flashing Chamber**

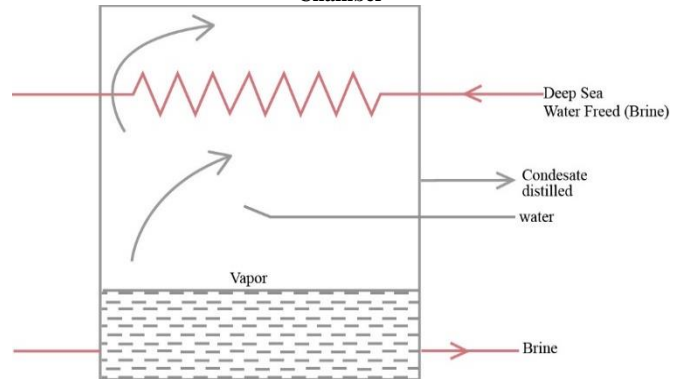


**Fig. 2 PV-Thermal integrated Flashing Chamber process.**

#### 3.1. Nanofluid Heat Transfer Fluid

Different equations have been reported in references [17-19] on calculating the specific heat, thermal conductivity, viscosity, and density using the law of mixtures. The thermophysical, thermodynamic, and heat transfer properties of nanofluids are determined in terms of the volumetric concentration of nanoparticles as per the following equation.

$$\alpha_{total} = \alpha_{particles} + \alpha_{base\ fluid} \quad (5)$$

Where  $\alpha$  represents the thermophysical property of a particular nanofluid.

The nanofluid thermal and thermophysical properties,  $\alpha_{total}$ , can be calculated as follows.

$$\alpha_{total} = \alpha_{base\ fluid} + \alpha_{particles} (\Phi) \quad (6)$$

Where  $\Phi$  represents the nano particles' volumetric concentration.

The thermal conductivity to thermal diffusivity and density of the nanofluids are related as follows [17-19];

$$\lambda = \alpha \delta C_p \quad (7)$$

Where  $C_p$  is the specific heat,  $\alpha$  is the thermal diffusivity, and  $\lambda$  and  $\rho$  represent the thermal conductivity and density, respectively.

Interested readers in further details about the calculations of the nanofluid's thermophysical and thermodynamic properties are advised to consult references [17-18, 20-21, 22-24]. In particular, these references discuss the impact of the nanofluids concentrations on the thermophysical properties of the said nanofluids. Moreover, the scope of this study is to discuss the MSF process using the PV-Thermal with nanofluids as heat transfer fluids and not to discuss the thermophysical properties of the nanofluids since they are discussed elsewhere; references [17-24].

#### 4. Magnetized Nanofluids

Equations (12) through (14) can be used to determine other thermophysical properties, such as;  $\alpha$  is the thermal diffusivity,  $\lambda$ , and  $\rho$  represent the thermal conductivity and density as different magnetic forces Gauss published in the literature properties ([9], [11], [21]) as a function of the properties outlined in the Table.1

Where “b” represents the nanofluid-specific property and “a” is the magnetic field force in Gauss.  $C_{pnf}$ ,  $K_{nf}$ , and  $h$  are the specific heat, thermal conductivity, and heat transfer coefficients of nanofluids.

Finally, the Availability and Irreversibility of the flashing process are discussed in the following.

$$A_q = \Sigma(1 - T_{amb}/T_j) Q_j \quad (8)$$

Where  $A_q$  is the flow availability change under steady-state conditions per stage and is the availability transfer due to  $Q_j$ , the heat transfer between the control volume and its surroundings,  $T_{amb}$  and  $T_j$  are the ambient temperatures and the flashing chamber temperature, respectively.

The availability destruction, i.e. irreversibility in the process per stage, can be determined from the following.

$$I_j = T_{amb} \times S_j \quad (9)$$

Where the  $S_j$  represents the entropy of the flashing process at each stage

#### 5. Thermal Storage

The proposed model is an extension of the model presented recently by Sami [29] based on the following assumptions: PCM is homogeneous and isotropic, HTF is incompressible, and it can be considered as a Newtonian fluid, inlet velocity and inlet temperature of the HTF are constant, PCM is in the solid phase for melting or in the liquid phase for solidification, thermophysical properties of the HTF and the PCM are constant. The phase change material experiences three phases; solid, liquid, and mushy. The solid and liquid phases have sensible heat additions, and the mushy has latent heat addition.

The conservation equations and heat transfer equations were written for each element/control volume of the PCM as follows for each of the phases of from solid, mushy, and liquid phases.

The heat released by the heat transfer fluid HTF by each tube is outlined in reference [29]; interested readers in developing the interaction during the thermal storage process to consult Sami [29].

##### 5.1. Discharge Phase

During the discharge process phase, the change material experiences a phase change from liquid to mushy and solid while yielding heat that is absorbed during the charging process. The water mass flow rate of heat transfer fluid during the discharge process is fully detailed in reference [29]. Interested readers are advised to consult Sami [29] for further details on modeling the discharge phase process.

#### 6. Numerical Procedure

The model describing the energy conversion process in the PV-Th panels, integrated desalination by flashing chamber process concept using nanofluids has been presented in Equation 1 through Equation 9. The flow diagram in Figure 3 has been established to solve the aforementioned system of mass and energy equations taking place during the flashing chamber and the thermal storage processes. The calculation starts with the input of the parameters of the PV-Thermal solar panel, thermal tubes, the PCM phase change, desalination chamber parameters, nanoparticles,  $Al_2O_3$ ,  $CuO$ ,  $Fe_3O_4$ , and  $SiO_2$ , and heat transfer fluid. The system equations have been integrated into the finite-difference formulations to determine the behavior of the process at each flashing chamber. Iterations were

performed using MATLAB iteration techniques until a converged solution was reached with less than 0.05. Solar radiation determines the mass flow rate of the nanofluid circulating in the thin tubes welded to the PV solar collector. Then the thermophysical properties and the heat transfer characteristics of the base fluid, water, and nanofluids at different concentrations are determined. In addition, mass and energy in the PCM thermal storage tank and the flashing chamber control volumes. This was accomplished by solving the finite-difference formulation of the aforementioned system of equations. Then the parameters describing the behavior of PV-Thermal solar panels, PCM phase change, and the flashing chamber process were determined under different conditions. Finally, the individual and hybrid system efficiencies, availability, and irreversibility, which represent the availability destruction in the process, were calculated.

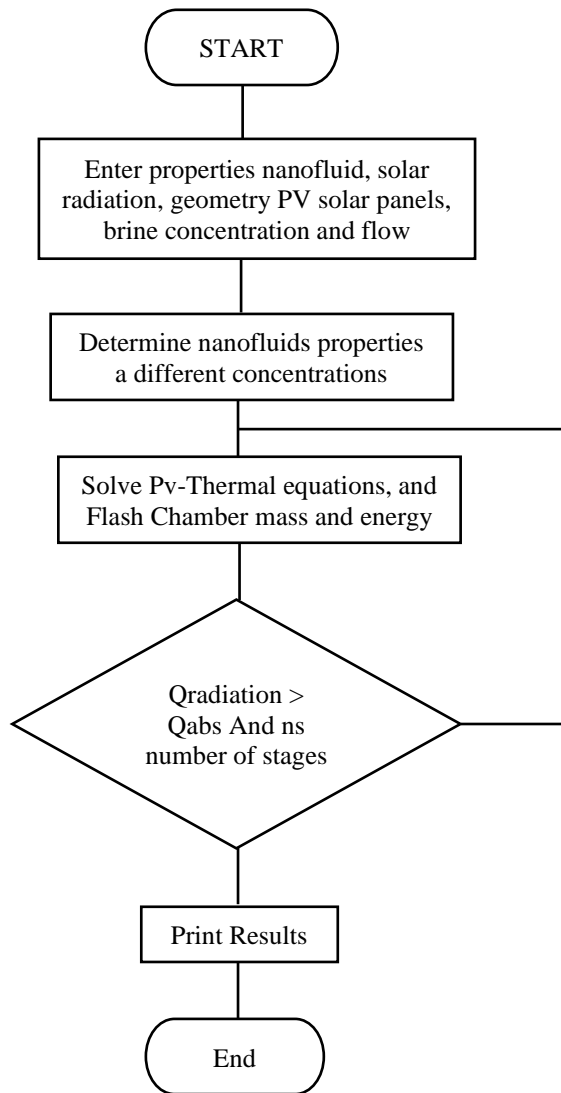


Fig. 3 Logic diagram for the numerical solution

### 7. Discussion and Analysis

The aforementioned system of equations (1) through (9) has been numerically solved in finite-difference formulation for the desalination flashing process using magnetized nanofluids at different concentrations, and the water was used as a base heat transfer fluid. In the following sections, the predicted results under different inlet conditions were present and discussed.

In particular, equations (1) through (4) have been solved to predict the photovoltaic-thermal solar panel hybrid system's dynamic total power generated and efficiencies. As reported and discussed by Sami ([16] through [18]), it is evident that the higher the solar radiations, the higher the thermal and hybrid efficiencies. It is also observed that the hybrid efficiency exhibits lower values than its thermal efficiency since the PV solar panel efficiency is significantly lower than the thermal efficiency. Also, the higher the solar radiation, the accelerated increase in the PV cell temperature. Consequently, it also shows that the higher the solar radiation, the higher the PV power and PV amperage.

Sami and others [16-18, 20 through 23] reported that nanofluids, such as CuO, Fe3O4, and SiO2, have received significant attention in the literature on the PV-Thermal hybrid system. It is also evident from the results presented in these references that the nanofluid CuO has the highest characteristic performance among the other nanofluids compared to water as base heat transfer fluid in the PV-Thermal solar collector system. This can be attributed to the higher thermodynamic, thermophysical, and heat transfer properties of the nanofluid CuO. Also, it has been reported that the PV-Thermal efficiency is enhanced with higher nanofluid concentrations at constant solar radiation.

On the other hand, ten flashing chambers were numerically simulated using equations (5) through (16). Where the brine flow is heated up in the preheater tank, as shown in the figure. 1. A salt concentration of 5% was used in the brine flow and 60 F ambient temperature. In addition, 100 PV solar panels were assumed with 300 watts per PV solar panel. Solar radiations were taken as 500 w/m2, 750 w/m2, 1000 w/m2, and finally, 1200 w/m2.

Since nanofluid Al2O3 is one of the most common nanofluids studied and reported in the literature, namely Sami{3}, Figure 4 demonstrates the impact of using this nanofluid at concentrations of 10% and 20% on the different behavior of the most important key parameters of the flashing process and also compared to water as a base fluid, at solar radiation of 500 w/m2. Examining these results suggests that the higher the nanofluid concentration as a heat transfer fluid, the lower the salt % in the flashed flow leaving the set of the flashing chambers compared to water as the base heat transfer fluid used in the brine preheater. Also,

Sami [3] and others reported that the higher the solar radiation, the lower the salt % in the flashed flow. This can be attributed to higher solar radiation, resulting in a higher temperature of the heat transfer fluid and the brine flow in the preheater entering the flashing chambers. Also, the higher the heat transfer fluid temperatures, the higher the brine flow temperatures and the higher the amount of distilled water evaporated or flashed. Moreover, it is also noted that the salt % in brine is increased progressively in the flashing chambers until reaching its maximum value at the final chamber.

Flashed Flows at different Gauss magnetic field predictions are shown in Figure 5, which displays the driving thermal energy to evaporate the flashed flow at each flashing chamber at different magnetized nanofluids  $Ai_2O_3$ ,  $CuO$ ,  $Fe_3O_4$ , and  $SiO_2$ . The flashed flow varies depending upon the nanofluids, and the magnetic Gauss field applied. It can be noted from Figures 4 and 5 that the flashed flow is reduced progressively and reaches its lowest value at the last flashing chamber. Thus, the amount of the produced distillate water, i.e. the amount of vapor extracted from brine, decreases along the stages and consequently along with the flashing conditions in each chamber: temperature and pressure. This is due to the increase in the heat of vaporization at lower saturation temperatures. Factually. In addition, the results also demonstrate that the higher the nanofluid concentration, the higher the flash flow produced during the flashing process compared to water as base fluid.

Figures. 6 and 7 display the flashed Flow at different magnetized nanofluids at 500 w/m<sup>2</sup> and 750 w/m<sup>2</sup> solar radiations and demonstrate that the higher the thermal energy driving the flashing evaporation inside the chambers, the higher the flashed flow across the board for all the magnetized nanofluids under investigation. However, the CU nanofluid appears to show a higher flash flow.

To study the influence of solar radiation on the flashed flow, Figure 8 has been constructed. There is clear evidence that the higher the solar radiation, the higher the flash flow produced. This was demonstrated at both concentrations of the magnetized nanofluids. Also, these figures show that magnetized nanofluids  $Ai_2O_3$  and  $Fe_3O_4$  produce the highest flashed flow among the nanofluids under investigation and water as the base fluid. This observation is significant since using the nanofluid  $Ai_2O_3$ , and  $Fe_3O_4$  can enhance the production of flashed flow three to four times over the water as a base fluid.

An irreversible process increases the entropy of the system in question. The second law of thermodynamics can be used to determine the irreversibility of a process as per the equation (16). In the thermodynamic process, the energy is lost to the surroundings in the form of Irreversible energy. However, the remaining amount of energy is defined as the

Available Energy in the process [20], [21]. This thermodynamic principle has been applied in the current study of the flashing chamber process and expressed in equations (15) and (16) to assess the lost and available energy. In particular, figures 9 through 12 demonstrate the irreversibility and availability of different magnetized nanofluids at solar radiation 1200 w/m<sup>2</sup> during the flashing process at each stage. The results are displayed in this figure.9 clearly shows that the irreversibility is reduced by using nanofluid  $Ai_2O_3$  at a higher concentration compared to water as a base fluid. Furthermore, the higher the concentration of  $Ai_2O_3$ , the higher the availability at the last flashing chamber. However, the availability is progressively reduced at the last flashing chamber.

Figures .9 through 15 explain the impact of the nanofluids' increase in nanofluids' concentrations on the irreversibility and availability of the desalination flashing process at 1200 w/m<sup>2</sup> solar radiation. The results presented in these figures clearly show that the type of nanofluids significantly influences the irreversibility. Also, as expected, the irreversibility increases progressively across the chambers till reaching a maximum at the last chamber. As reported by [20] and [21], the highest irreversibility was experienced when water was used as a base fluid, and the lowest irreversibility was associated with nanofluid  $SiO_2$ . The irreversibility increase depends upon the type of nanofluid and its thermodynamic properties. Also, it appears that the nanofluid concentration does not significantly impact the changes of irreversibility across the various chamber during the flashing process.

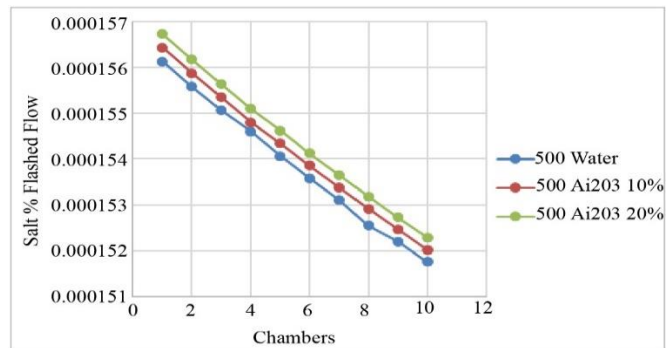


Fig. 4 Salt % in flashed Flow at 500 w/m<sup>2</sup>

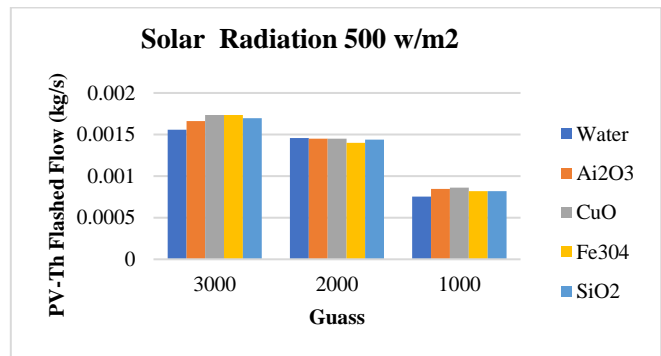


Fig. 5 Flashed Flow at different magnetic fields

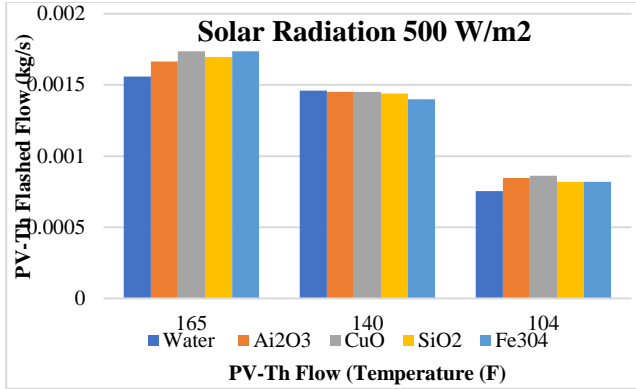


Fig. 6 Flashed Flow at different temperatures

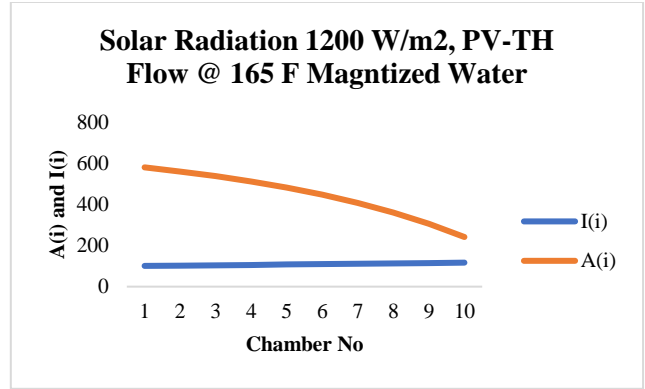


Fig. 10 Magnetized Water Irreversibility and availability at 1200 w/m2

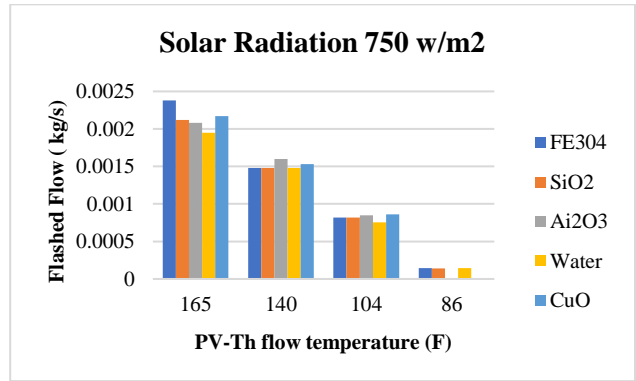


Fig. 7 Flashed Flow at different magnetized nanofluids

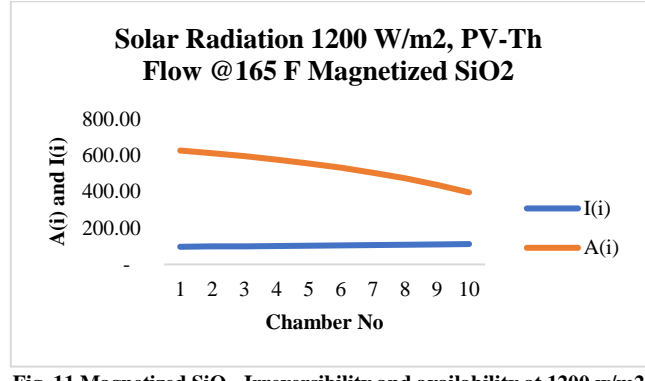


Fig. 11 Magnetized SiO<sub>2</sub> Irreversibility and availability at 1200 w/m2

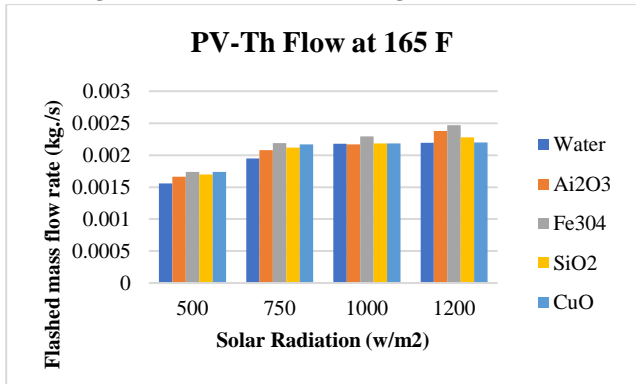


Fig. 8 Flashed Flow at different solar radiations

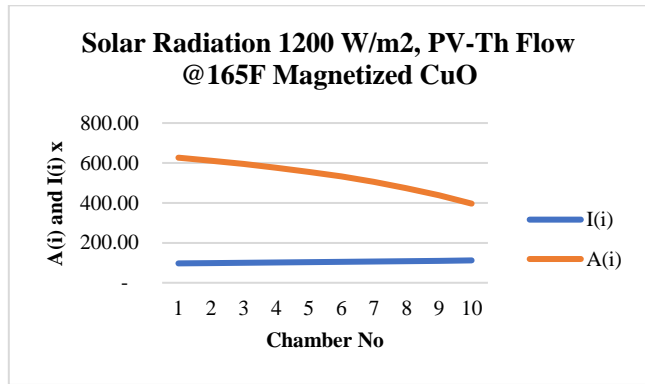


Fig. 12 Magnetized CUO Irreversibility and availability at 1200 w/m2

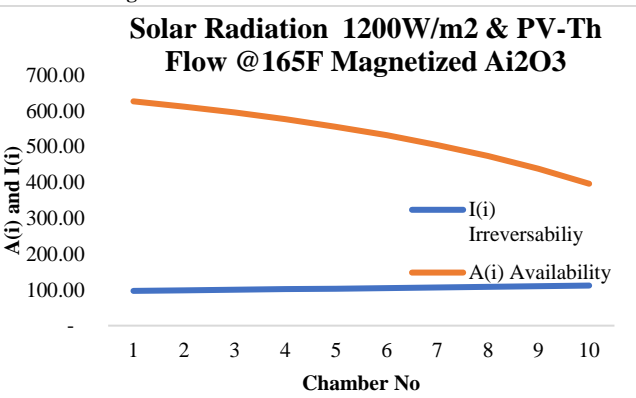


Fig. 9 Magnetized Ai<sub>2</sub>O<sub>3</sub> Irreversibility and availability at 1200 w/m2

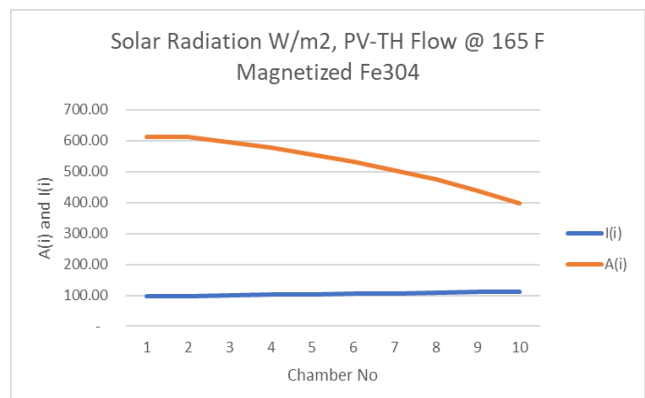


Fig. 13 Magnetized Fe304 Irreversibility and availability at 1200 w/m2

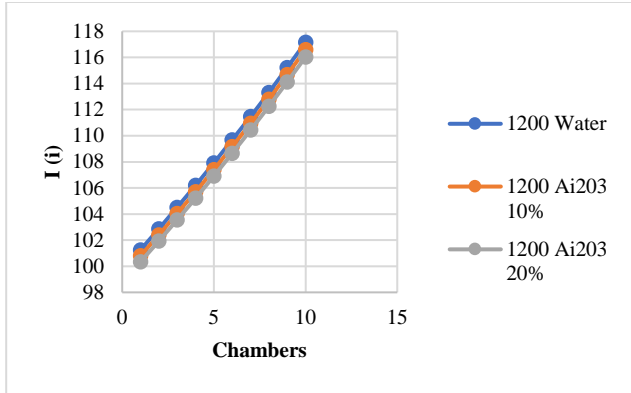


Fig. 14 Irreversibility at 1200 w/m2

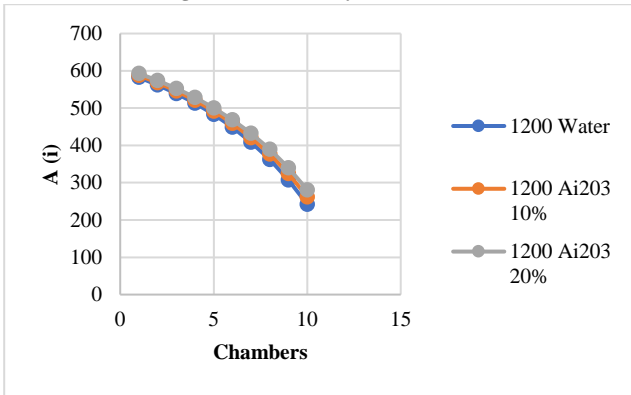


Fig. 15 Availability at 1200 w/m2

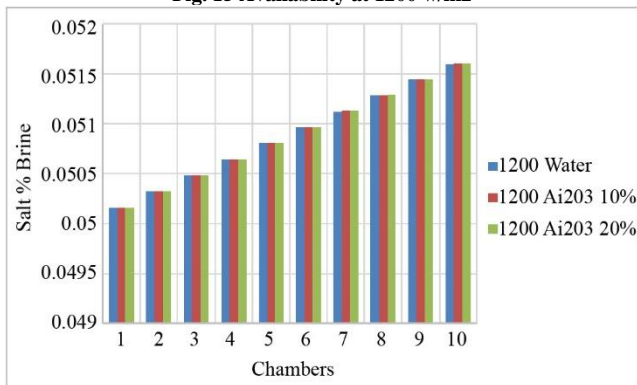


Fig. 16 Salt % in brine at 1200 w/m2

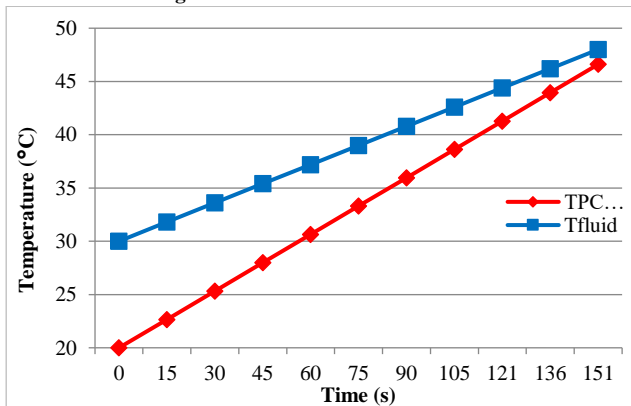


Fig. 17 Thermal storage temperature gradients under 550 w/m2

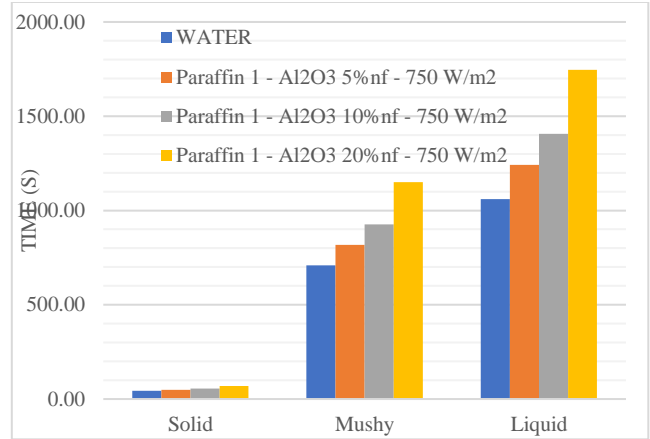


Fig. 18 Comparison of time during the phase change material process with Al2O3

The nanofluid's thermal storage thermophysical and thermal properties with various volumetric concentrations were calculated using equations (17) through (24). Including the thermal storage tank, the present model, as shown in Figures 1 and 2, is very crucial to the operation of the solar desalination 24/7 system even with cloudy and low sunshine solar radiation days. The prediction of the thermal storage behavior using typical nanofluids  $Al_2O_3$  at different concentrations is shown in the figure. 16 through Figure .18, where the time consumed at solar radiation 750 w/m2 by the phase change material process during the different phases: solid, mushy, and liquid phase change while implementing  $Al_2O_3$  nanofluid as heat transfer fluid at different concentrations from 5 to 20 %. Moreover, it also appeared from the data displayed in these figures that the thermal energy storage time required for phase change was significantly dependent on the concentration of nanofluid  $Al_2O_3$  and the phase change material. This phenomenon has been reported by other references, particularly reference [21] for other nanofluids.

On the other hand, it can be observed from the discussion mentioned above ( Cf. Figure 16) that the Salt percentage in the brine flow at 1200 w/m2 was increased progressively across the chambers with the use of the nanofluids; however, the concentration of the nanofluid slightly impacted the increase of the percentage of salt in the brine flow. In addition, the results plotted in these figures show that the Salt percentage in the brine flow was independent of the type of nanofluids among the water as a base fluid, as reported in [3].

Also, the availability determined by equation (15) diminishes progressively along the flashing chambers and reaches the lowest value at the last chamber. It also appears from Figures 14 and 15 that the nanofluid concentrations have a limited impact on the availability during the process of the flashing. On the other hand, Figures 14 and 15 display

the development of the flashed flow at different chambers. In general, the data in these figures show that the flashed flow is progressively reduced until it reaches the lowest value at the last chamber. This is due to the increased heat of vaporization at lower saturation temperatures; therefore, less vapor is extracted from brine. As expected, the data show that the higher the nanofluid concentration, the higher the amount of flashed flow produced.

Further analysis of the observed data demonstrates that the nanofluid  $\text{Al}_2\text{O}_3$  produces the highest amount of flashed flow during this process. Their impact on the pump power was considered while calculating the Availability and Irreversibility of the flashing process. Finally, it is worthwhile mentioning that lower nanofluids concentrations did not yield higher thermal capacities needed for the flashing process of the brine,

## 8. Model Validation

Very limited experimental data was published on the low-temperature desalination by flashing technique. However, to our best knowledge, none was available using nanofluids. Therefore, the data published by Nannaronea et al. [7] was used in this study for validation purposes. Figure. 19 has shown a comparison between results predicted by this model for the low-temperature flashed flow and the data reported in reference [7]. As can be observed from this figure that the amount of the produced distillate decreases along the stages progressively and consequently as the flash temperature and pressure decrease profiles. This is due to the increased heat of vaporization at lower saturation temperatures; therefore, less vapor is extracted from brine.

This figure depicts the flashed flow reduction ratio across the flashing chambers from the first to the last chamber. The data reported by reference [7] on the reduction ratio of the flashed flow was compared to the predicted results chamber by chamber. The comparison clearly shows that the model compared well with the data. However, the data was underpredicted. This can be attributed to the energy lost to the surroundings in the form of Irreversible energy during the flashing process taking place in each chamber and was not fully taken into account by the mass and energy balances built in the present model, as can be seen in equation (16).

The thermal storage model presented hereby has been validated against the experimental data reported by Abdulateef et al. [30] during the phase change melting process using  $\text{Al}_2\text{O}_3$  nanoparticles to enhance the thermal conductivity and other thermophysical properties of the heat transfer fluid, as shown in Figure.20. The comparison displayed in Figure.19 proved the reliability of the thermal energy storage model presented hereby and in fair agreement with the data presented in Figure .20.

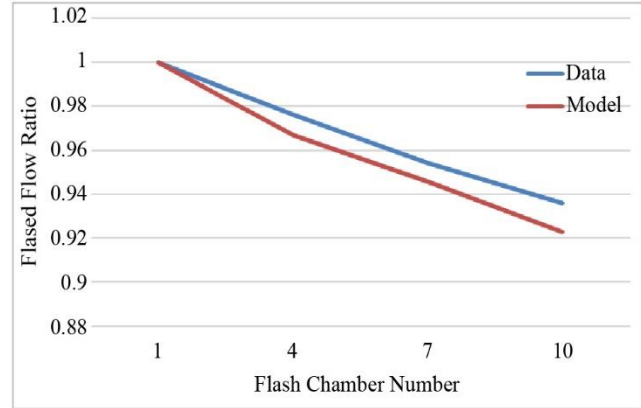


Fig. 19 Comparison between model prediction and data [7].

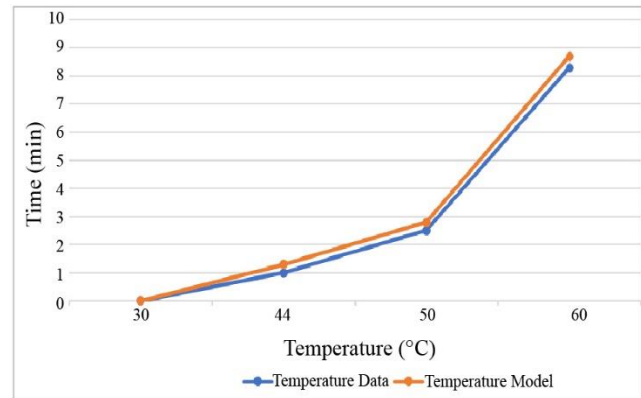


Fig. 20 Comparison between model prediction and data reference [30]

## 9. Conclusion

A mathematical and numerical model was presented to describe the PV-thermal solar to power the multi-stage flashing chamber process using magnetized nanofluids and an integrated thermal storage tank with paraffin wax as PSM. The model proposed has been established after the mass and energy conservation equations were written using the control volume approach and integrated with thermal and thermophysical properties of the water and magnetized nanofluids as heat transfer fluids in the PV-Thermal solar system. The magnetized nanofluids studied are  $\text{Al}_2\text{O}_3$ ,  $\text{CuO}$ ,  $\text{Fe}_3\text{O}_4$ , and  $\text{SiO}_2$ . The flashing process has been studied under various conditions, including different solar radiations, brine concentrations, magnetized nanofluids concentrations, and flashing chamber temperatures. Solar radiations were taken as  $500 \text{ w/m}^2$ ,  $750 \text{ w/m}^2$ ,  $1000 \text{ w/m}^2$ , and  $1200 \text{ w/m}^2$ . The magnetized nanofluids volumetric concentrations considered varied from 1% to 20%.

There is clear evidence that the higher the solar radiation and the higher the magnetic field Gauss, the higher the flash flow produced. The results also clearly show that the irreversibility is reduced by using nanofluid  $\text{Al}_2\text{O}_3$  at a higher concentration of 10% to 20% compared to water as a base fluid. The highest irreversibility was experienced when water was used as a base fluid, and the lowest irreversibility

was associated with nanofluid SiO<sub>2</sub>. The irreversibility increase depends upon the type of nanofluid and its thermodynamic properties. Furthermore, the higher the concentration of Al<sub>2</sub>O<sub>3</sub>, 10% to 20%, the higher the availability at the last flashing chamber. However, the availability is progressively reduced at the last flashing chamber. It was observed that the nanofluid SiO<sub>2</sub> has the highest availability among the other nanofluids and water as based fluid across the flashing chambers.

The results demonstrated that it is possible to increase the preheating process quality by increasing the flashing chamber temperature, which improves the plant's thermal efficiency. The present study demonstrated an added value to the research in thermal desalination through the use of solar energy, solar PV-Thermal panels, as the driving force to the evaporation process. This approach represents a step toward sustainability and reducing global warming effects. The predicted results were compared to experimental data published in the literature. The comparison showed that the model fairly predicted the data under consideration. Finally, we believe that future studies should look into other nanofluids as well as different concentrations at different salt concentrations.

## References

- [1] Paul Byrne et al., "A Review of the Coupling of Cooling, Desalination, and Solar Photovoltaic Systems," *Renewable and Sustainable Energy Reviews*, vol. 47, pp. 703-717, 2015. *Crossref*, <https://doi.org/10.1016/j.rser.2015.03.083>
- [2] ALli M. El-Nashar, "The Economic Feasibility of Small Solar MED Seawater Desalination Plants for Remote Arid Areas," *Desalination*, vol. 134, no. 1-3, pp. 173-186, 2001. *Crossref*, [https://doi.org/10.1016/S0011-9164\(01\)00124-2](https://doi.org/10.1016/S0011-9164(01)00124-2)
- [3] Samuel Sami, "Study of the Impact of PV-Thermal and Nanofluids on the Desalination Process by Flashing," *Applied System Innovation*, vol. 3, no. 1, 2020. *Crossref*, <https://doi.org/10.3390/asi3010010>
- [4] V.Velmurugan, S. Prem Kumar, and S. Ragul, "Humidification-Dehumidification Desalination System - An Overview," *International Journal of Scientific Research in Science and Technology*, vol. 5, no. 4, pp. 1163-1177, 2018. *Crossref*, <https://ijrst.com/paper/4136.pdf>
- [5] Ange Abena Mbarga et al., "Integration of Renewable Energy Technologies, With Desalination," *Current Sustainable Renewable Energy Report*, vol. 1, pp. 11-18, 2014. *Crossref*, <https://doi.org/10.1007/s40518-013-0002-1>
- [6] Mohamed A. Sharaf Eldean, "Design and Simulation of Solar Desalination Systems," Energy Engineering to Faculty of Petroleum & Mining Engineering Suez Canal University, Egypt, 2011.
- [7] Devesh Singh, and Freddie L. Inambao, "Solar Desalination: A Critical Review," *International Journal of Mechanical Engineering and Technology (IJMET)*, vol. 10, no. 8, pp. 244-270, 2019.
- [8] Hazim Mohamed Qiblawey, and Fawzi Banat, "Solar Thermal Desalination Technologies," *Desalination*, vol. 220, no. 1-3, pp. 633-644, 2008. *Crossref*, <https://doi.org/10.1016/j.desal.2007.01.059>
- [9] Mohamed A. Eltawil, Zhao Zhengming, and Liqiang Yuan, "A Review of Renewable Energy Technologies Integrated with Desalination Systems," *Renewable and Sustainable Energy Reviews*, vol. 13, no. 9, pp. 2245-2262, 2009. *Crossref*, <https://doi.org/10.1016/j.rser.2009.06.011>
- [10] Chennan Li, Yogi Goswami, and Elias Stefanakos, "Solar Assisted Seawater Desalination: A Review," *Renewable and Sustainable Energy Reviews*, vol. 19, pp. 136-163, 2013. *Crossref*, <https://doi.org/10.1016/j.rser.2012.04.059>
- [11] Soteris A. Kalogirou, "Solar Thermal Collectors and Applications," *Progress in Energy and Combustion Science*, vol. 30, no. 3, pp. 231-295, 2004. *Crossref*, <https://doi.org/10.1016/j.peccs.2004.02.001>
- [12] K. Trivedi Hetal, D.B. Upadhyay, and A.H. Rana, "Seawater Desalination Process," *International Journal Of Engineering Sciences & Research Technology*, vol. 3, no. 2, pp. 638-646, 2014.
- [13] Bakhodir Abdullayev et al., "Lithium Recovery from Water Resources by Membrane and Adsorption Methods," *International Journal of Engineering Trends and Technology*, vol. 70, no. 9, pp. 319-329, 2022. *Crossref*, <https://doi.org/10.14445/22315381/IJETT-V70I9P231>
- [14] Hala Faisal Al-Fulaij, "Dynamic Modeling of Multistage Flash (MSF) Desalination Plan," University College London (UCL), 2011.
- [15] A.O. Bin Amer, "Development and Optimization of ME-TVC Desalination System," *Desalination*, vol. 249, no. 3, pp. 1315-1331, 2009. *Crossref*, <https://doi.org/10.1016/j.desal.2009.06.026>

## Acknowledgement

The research work presented in this paper was made possible through the support of transpacific Energy, Inc.

## Nomenclature

- C<sub>p</sub> the specific heat kJ/kg k  
 H enthalpy kJ/kg  
 I<sub>j</sub> Irreversibility kJ/kg  
 m mass flow rate kg/s  
 Q<sub>in</sub>: Energy received due to solar irradiation,  
 Q<sub>conv</sub>: Energy loss due to Convection  
 Q<sub>elect</sub>: Electrical power generated  
 S<sub>c</sub> salt concentration, g/kg  
 S<sub>j</sub> is the entropy of the flashing process at each stage KJ/kg.  
 K  
 S<sub>p</sub>: Total area of the PV module  
 t: time
- T<sub>j</sub> Flashing chamber temperature, K  
 T<sub>amb</sub> ambient temperature  
 Greek Symbols:  
 α the thermal diffusivity  
 Φ the nano particles volumetric concentration.  
 ρ density, kg/m<sup>3</sup>

- [16] Tarek H. Nigim, “Computational Modeling of Thermofluidic Flashing in MSF Desalination,” The National University of Ireland as the fulfillment of the requirements for the Degree of Doctor of Philosophy, Department of Mechanical Engineering National University of Ireland, Galway, 2017.
- [17] A.E. Kabeel, and Emad M.S. El-Said, “Applicability of Flashing Desalination Technique for Small Scale Needs Using a Novel Integrated System Coupled with Nanofluid-based Solar Collector,” *Desalination*, vol. 333, no. 1, pp. 10–22, 2014. *Crossref*, <https://doi.org/10.1016/j.desal.2013.11.021>
- [18] Kapil Garg et al., “Performance Evaluation of a Brine-recirculation Multistage Flash Desalination System Coupled with Nanofluid-based Direct Absorption Solar Collector,” *Renewable Energy*, vol. 122, pp. 140-151, 2018. *Crossref*, <https://doi.org/10.1016/j.renene.2018.01.050>
- [19] D.J. Yang et al., “Simulation and Experimental Validation of Heat Transfer in a Novel Hybrid Solar Panel,” *International Journal of Heat and Mass Transfer*, vol. 55, no. 4, pp. 1076-1082, 2012. *Crossref*, <https://doi.org/10.1016/j.ijheatmasstransfer.2011.10.003>
- [20] Branislav Lalovi, Zoltan Kiss, and Herbert Weakliem, “Hybrid Amorphous Silicon photovoltaic and Thermal Solar-collector,” *Solar Cells*, vol. 19, no. 2, pp. 131–138, 1986. *Crossref*, [https://doi.org/10.1016/0379-6787\(86\)90038-4](https://doi.org/10.1016/0379-6787(86)90038-4)
- [21] S. Sami, “Prediction of Performance of a Novel Concept of Solar Photovoltaic-Thermal Panel and Heat Pipe Hybrid System,” *International Journal of Modern Studies in Mechanical Engineering (IJMSME)*, vol. 5, no. 1, pp. 1-8, 2019. *Crossref*, <http://dx.doi.org/10.20431/2454-9711.0501001>
- [22] S. Sami, and C. Campoverde, “Dynamic Simulation and Modeling of a Novel Combined Hybrid Photovoltaic-Thermal Panel Hybrid System,” *International Journal of Sustainable Energy and Environmental Research*, vol. 7, no. 1, pp. 1-23, 2018.
- [23] Samuel M. Sami, and E. Marin, “Modelling and Simulation of PV Solar-Thermoelectric Generators using Nano Fluids,” *International Journal of Sustainable Energy and Environmental Research*, vol. 8, no. 1, pp. 70-99, 2019. *Crossref*, <http://dx.doi.org/10.18488/journal.13.2019.81.70.99>
- [24] Christopher Allen, “Magnetic Field Enhancement Thermal Conductivity Analysis of Magnetic Nanofluids,” MSc, The University of Texas at Arlington, 2015.
- [25] Ali H.A. Al-Waelia et al., “Numerical Study on the Effect of Operating Nanofluids of the Photovoltaic Thermal System (PV/T) on the Convective Heat Transfer,” *Case Studies in Thermal Engineering*, vol. 12, pp. 405–413, 2018. *Crossref*, <https://doi.org/10.1016/j.csite.2018.05.011>
- [26] Suman Saha, M.R.I Sarker, and S.S. Tuly, “Performance Study of a Water Desalination System Under Vacuum,” *SSRG International Journal of Mechanical Engineering*, vol. 7, no. 8, pp. 18-22, 2020. *Crossref*, <https://doi.org/10.14445/23488360/IJME-V7I8P103>
- [27] S. Sami, “Modelling and Simulation of Performance of Nanofluids in PV-Thermal Solar Panel Collectors,” *Ra Journal Of Applied Research*, *Crossref*, <https://doi.org/10.31142/rajar/v5i1.07>
- [28] Michael John Moran, *Fundamentals of Engineering Thermodynamics*, John Wiley & Sons, Inc., USA, 2014.
- [29] Valery Ya. Rudyak, and Andrey V. Minakov, “Thermophysical Properties of Nanofluids,” *The European Physical Journal*, vol. 41, 2018. *Crossref*, <https://doi.org/10.1140/epje/i2018-11616-9>
- [30] Samuel Sami Howard, “Numerical Modeling Prediction of Thermal Storage During Discharging Phase, PV- Thermal Solar and with Nanofluids,” *Journal of Technology Innovations in Renewable Energy*, vol. 10, 1-18, 2021. *Crossref*, <https://doi.org/10.6000/1929-6002.2021.10.01>
- [31] Ammar M. Abdulateef et al., “Thermal Performance Enhancement of Triplex Tube Latent Thermal Storage Using Fins-Nano- Phase Change Material Technique,” *Heat Transfer Engineering*, vol. 39, no. 12, pp. 1067-1080, 2018. *Crossref*, <https://doi.org/10.1080/01457632.2017.1358488>
- [32] Alessandro Nannaronea, Claudia Torob, and Enrico Sciubba, “Multi-Stage Flash Desalination Process: Modeling and Simulation,” *Proceedings of Ecos 2017 - The 30th International Conference on Efficiency, Cost, Optimization, Simulation and Environmental Impact of Energy Systems*, San Diego, California, 2017.